Carbon Letters (2020) 30:73–80
https://doi.org/10.1007/s42823-019-00072-6

Online ISSN 2233-4998
Print ISSN 1976-4251

ORIGINAL ARTICLE

Electrochemical characterization of reduced graphene oxide as an ion-to-electron transducer and application of screen-printed all-solid-state potassium ion sensors

Jo Hee Yoon[1] · Hong Jun Park[1] · Seung Hwa Park[1] · Kyoung G. Lee[2] · Bong Gill Choi[1]

Received: 16 May 2019 / Revised: 9 July 2019 / Accepted: 11 July 2019 / Published online: 25 July 2019

Abstract
We report potentiometric performances of ion-to-electron transducer based on reduced graphene oxide (RGO) for application of all-solid-state potassium ion sensors. A large surface area and pore structure of RGO are obtained by a hydrothermal self-assembly of graphene oxide. The extensive electrochemical characterization of RGO solid contact at the interface of ion-selective membrane and gold electrode shows that the potassium ion-selective electrode based on RGO had a high sensitivity (53.34 mV/log[K^+]), a low detection of limit (− 4.24 log[K^+], 0.06 mM) a good potential stability, and a high resistance to light and gas interferences. The potentiometric K^+-sensor device was fabricated by combining of screen-printed electrodes and a printed circuit board. The K^+-sensor device accurately measures the ion concentration of real samples of commercial sports drinks, coke and orange juice, and then transfers the collected data to a mobile application through a Bluetooth module. The screen-printed ion sensors based on RGO solid contact show a great potential for real-time monitoring and point-of-care devices in human health care, water-treatment process, and environmental and chemical industries.

Keywords Ion sensor · Reduced graphene oxide · Potentiometry · Solid contact · Screen printing

1 Introduction

Potentiometric ion sensors, which consist of ion-selective and reference electrodes, can convert the concentration of target ions into a measurable signal of electrical potential [1]. Compared to conventional liquid-contact ion-selective electrodes with an inner filling solution, all-solid-state ion-selective electrodes show more benefits in mechanical flexibility, maintenance, operation, durability, and miniaturization, and thus present a promising range of potential applications in diagnostics, healthcare, and point-of-care devices [2–5]. However, applications with a small sample volume in limited spaces require an enhancement in sensor performances, such as reproducibility, potential stability, and detection limit [6–8]. As an ion-to-electron transducer, solid contact materials, which are generally placed at the interface of an electronic metal conductor and ion-selective polymer membrane, are regarded as an essential component for enhancing stable and reliable potentiometric ion sensors [1, 9]. Highly capacitive materials have been widely used as ion-to-electron transducers, including conducting polymers of polypyrrole [10], poly(3-octylthiophene) [11], polyaniline [12], poly(3,4-ethylenedioxythiophene) [3], and nanocarbons of carbon nanotubes [13], fullerene [14], graphene [8, 15, 16], and porous carbons [17, 18]. Although conducting polymers are effective ion-to-electron transducers, they suffer from the formation of the water layer and interferences from light and dissolved gases of O_2 and CO_2, which may cause unstable potential responses and severe potential drifts [9].

The electrical double-layer capacitive carbon materials have also been used as ion-to-electron transducers [8, 13–18]. Compared to conducting polymers, carbon materials

Jo Hee Yoon and Hong Jun Park have contributed equally to this work.

✉ Kyoung G. Lee
kglee@nnfc.re.kr

✉ Bong Gill Choi
bgchoi@kangwon.ac.kr

[1] Department of Chemical Engineering, Kangwon National University, 346 Joongang-ro, Samcheok, Gangwon-do 25913, Republic of Korea

[2] Nano-bio Application Team, National Nanofab Center, 291 Daehak-ro, Yuseong-gu, Daejeon 34141, Republic of Korea

show a promising possibility to improve the abovementioned issues of the water layer and interference of gases and potential stability due to the hydrophobicity and high specific capacitance of nanocarbon materials [13, 14]. Graphene is a single layer of carbon atoms arranged in a two-dimensional hexagonal lattice, showing unique thermal, optical, mechanical, electronic, and electrochemical properties [19]. Since graphene oxide (GO) has been synthesized via the chemical oxidation of graphite, RGO, which is simply obtained by the reduction of GO, has attracted much attention in terms of mass production, solution process, and the easy modification of graphene surface [20]. A high electrical double-layer capacitance of RGOs has made them an attractive ion-to-electron transducer for all-solid-state solid-contact ion-selective electrodes [15]. In particular, when RGO has a higher surface area with a porous structure, RGO provides more stable potential signals in a prolonged period of time and much lower sensitivity to light, oxygen, and carbon dioxide [16]. However, most RGO-based materials derived from GOs still remain a challenge; RGOs are aggregated during the conversion of GOs into RGOs, resulting in a decrease of surface area [21].

With the development of printing technology, printed electrochemical devices have gained a great deal of attention because of their mass production, low cost, and reproducibility [22]. Here, we report a miniaturized potentiometric ion-sensor device combining an all-solid-state ion-selective electrode and a reference electrode based on screen-printed silver electrodes. Three-dimensional (3D) RGO hydrogels were used as a solid-contact material, showing a Nernstian response, excellent potential stability, and a good resistance to the water layer and interference from light, O_2, or CO_2. As a proof of concept, a potassium ion sensor device was fabricated and integrated with a printed circuit board. The collected data were transferred through Bluetooth module and were then displayed in a mobile application. The potassium ion sensor provided accurate and reliable potential signals. Furthermore, the developed ion sensors could selectively measure the concentration of potassium ions in real food samples.

2 Experimental

2.1 Materials

Graphite powder (< 20 μm), ethylene diamine, valinomycin (potassium ionophore I), potassium tetrakis(4-chlorophenyl) borate (KTClPB), poly(vinyl chloride) (PVC), bis(2-ethylhexyl)sebacate (DOS), potassium chloride, sodium chloride, calcium chloride, magnesium chloride ammonium chloride, Sulfuric acid, 1-Methyl-2-pyrrolidinone (NMP), Tetrahydrofuran (THF) and Butvar® B-98 (PVB) was purchased from Sigma-Aldrich.

2.2 Preparation of RGO hydrogel

The RGO hydrogel was prepared by self-assembly of GO solution as follows. The 8 mL of GO solution (3 mg/mL) with 20 μM of ethylenediamine was placed in a Teflon autoclave, and the heated at 180 °C for 12 h. The resultant RGO hydrogels were washed with deionized (DI) water and ethanol several times, and were then stored in DI water.

2.3 Preparation of ISM–RGO/Au electrode

The ISM–RGO/Au electrode was prepared using a drop-casting method as follows. A piece of RGO hydrogel was sonicated in NMP, and was then dropped onto the surface of Au electrode. The resultant RGO/Au was dried at 80 °C under vacuum for overnight. The potassium ion-selective membrane (ISM) was prepared by mixing of valinomycin (2 mg), KTClPB (0.5 mg), DOS (64.7 mg), and PVC (32.8 mg) in THF (1 mL). The K^+ selective membrane was drop-casted onto the surface of RGO/Au electrode at room temperature, and repeated three times to prepare ISM–RGO/Au electrodes. As a control sample, ISM/Au electrode was prepared without deposition of RGO.

2.4 Fabrication of a screen-printed K^+-sensor

The K^+-sensing electrode part of the silver screen-printed platform was manufactured in the same procedure as the ISM–RGO/Au electrode. The reference electrode was prepared by an electrolytic deposition of chloride at an applied constant voltage of 0.2 V for 400 s in 0.1-M KCl solution using three-electrode system.

2.5 Characterization

SEM image was performed by a field emission scanning electron microscope (S-4800). High and low resolution of TEM images were investigated by a field emission transmission electron microscope (JEM2100F, JEOL Ltd., Tokyo, Japan) operated at 200 kV. XRD data were investigated by a RigakuD/MAX-2500 (40 kW, Tokyo, Japan) with a θ/θ goniometer. XPS data were obtained on Thermo MultiLab 20000 (Thermo Fisher Scientific, Daejeon, Korea). The specific surface area was determined by N_2 adsorption/desorption measurement (ASAP-2010 surface area analyzer) using Brunauer–Emmett–Teller (BET) method. Potentiometry, cyclic voltammetry, amperometry, and chronopotentiometry were measured using CHI 760E (CH Instruments, Inc.). For a three-electrode system, ISM–RGO/Au, Ag/AgCl, and Pt wire were used as working, reference, and counter

electrodes, respectively. K^+-sensor has a two-electrode system consisting of ISM–RGO/Ag and Ag/AgCl reference electrodes. The gas layer test of ISM–RGO/Au electrode immersed in 0.1-M KCl solution was performed by continuously flowing N_2, O_2 and CO_2 gas (purity 99.9%). Real-sample measurements using screen-printed K^+ sensor were measured by Arduino-based PCB including 3.7 V Li-ion battery as a power source and a FBL780 Bluetooth module for data transmission.

3 Results and discussion

The 3D RGO hydrogels were prepared by a hydrothermal reduction method using a mixture of GO (3 mg/mL) and ethylene diamine (20 µM) in a Teflon-lined autoclave at 180 °C for 12 h. A self-assembled RGO monolith was obtained after cooling the autoclave at room temperature (Fig. 1a). This self-assembled hydrothermal reduction for fabricating 3D RGO hydrogels is a straightforward, simple, and one-step method with a low-cost and effective process. As the reduction of GO was processed, the oxygenated groups were removed from the GO surface, and π–π stacking between the 2D sheets and hydrophobicity was increased [23]. The increased π–π stacking and hydrophobicity lead to a self-assembly of 3D RGO hydrogel. Observation with SEM revealed that the exfoliated RGO sheets were interconnected with each other, thus showing a 3D porous structure with sub-micro-size pores (Fig. 1b, c). To investigate the TEM measurement, a piece of 3D RGO hydrogel was obtained using a sonicator and then dropped it onto a TEM grid. The TEM image shows an exfoliated and wrinkled RGO sheet, indicating no aggregation during the hydrothermal reduction of GO (Fig. 1d, e). Based on the BET method, 3D RGO hydrogel has a high specific surface area of 247 m^2/g (Fig. 1f). Furthermore, an X-ray powder diffraction (XRD) measurement confirmed the exfoliated state of 3D RGO. Compared to pristine graphite, the 2D spacing peak at 24° was dramatically reduced after hydrothermal reduction (Fig. 1g). The chemical reduction degree of GO was demonstrated by investigating the change of chemical state of GO and RGO sheets using an X-ray photoelectron spectroscopy (XPS) analysis technique (Fig. 1h). The C 1s XPS spectrum of GO showed two overlapped peaks that can be deconvoluted into four peaks, corresponding to C=C (284.4 eV), C–O (286.9 eV), C=O (288.7 eV), and COOH (292.4 eV), respectively. After hydrothermal reduction, the intensities of oxygenated group peaks were significantly decreased, indicating the formation of RGO.

The RGO electrode with a high surface area provides a high electrical double-layer capacitance, which is essential for effective solid-contact transducers. A cyclic voltammetry (CV) measurement was performed to investigate the electrical double-layer capacitance of RGO electrodes using a three-electrode system (Fig. 2a). The CV curve obtained for the RGO electrode was measured at a scan rate of 50 mV/s in a potential range of 0.0–1.0 V. The rectangular and symmetric CV shape indicates a well-defined electrical double-layer behavior of carbon materials. The

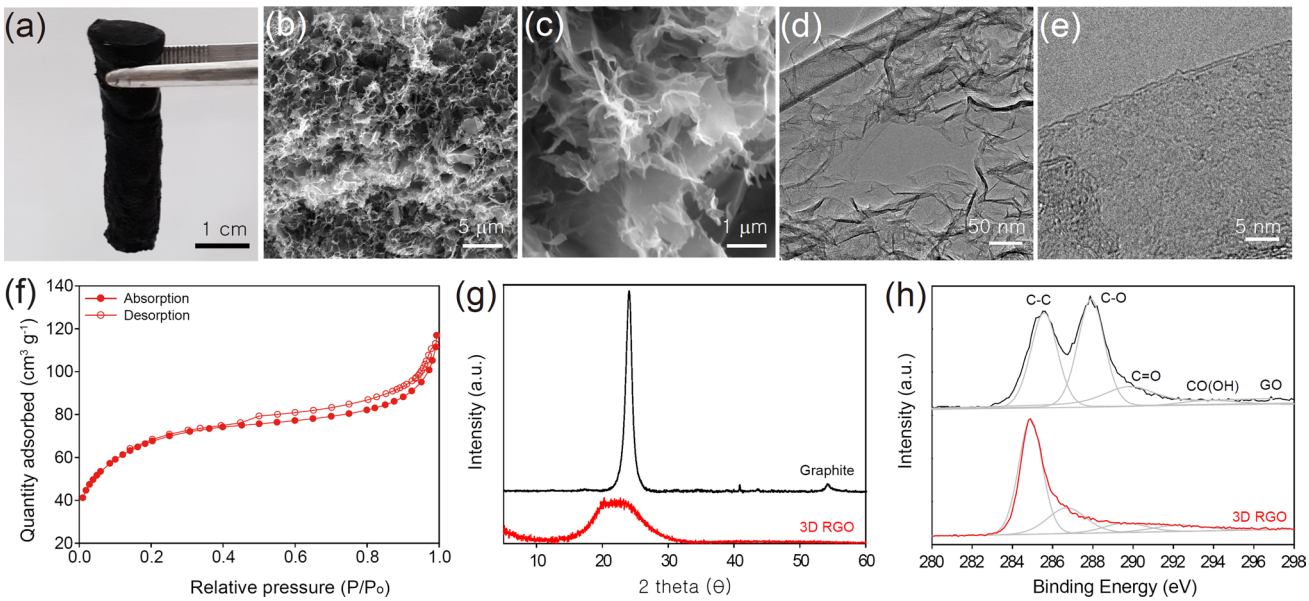

Fig. 1 **a** Photograph of 3D RGO hydrogel. **b**, **c** SEM and **d**, **e** TEM images of 3D RGO hydrogel. **f** N_2 adsorption/desorption isotherm of 3D RGO hydrogel. **g** XRD patterns of graphite and 3D RGO. **h** C 1s XPS spectra of GO and 3D RGO

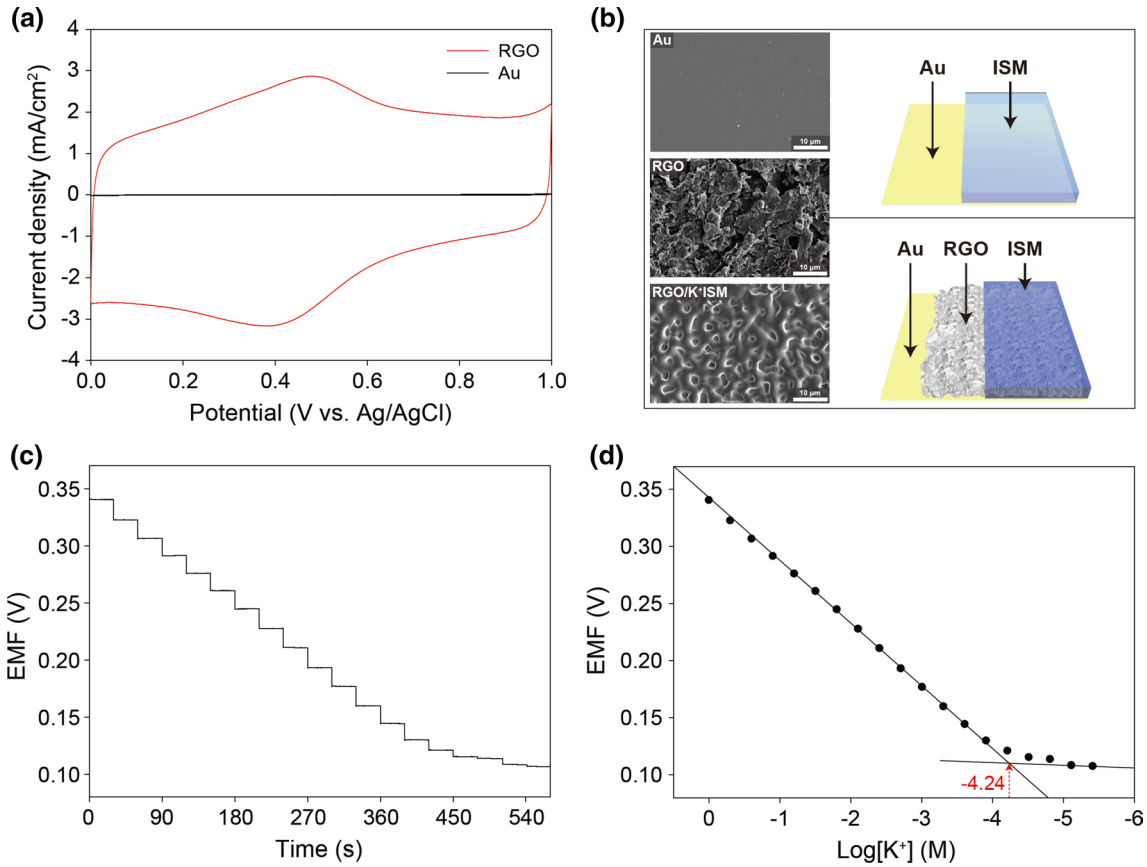

Fig. 2 **a** CV curves of RGO and Au electrodes at a scan rate of 50 mV/s in 1-M H_2SO_4 electrolyte. **b** SEM images of Au, RGO and ISM–RGO with schematic illustrations of ISM/Au and ISM–RGO/Au electrodes. **c** EMF responses of the ISM–RGO/Au electrode according to decreasing KCl concentration in a range of 0 to − 5.41 log[K^+]. **d** A plot of EMF versus log[K^+] for ISM–RGO/Au electrode

area capacitance (C_F) values can be calculated from CV curves using the following equation [24]:

$$C_F = \frac{2\int_o^t IU\mathrm{d}t}{U^2\left|\begin{matrix}U_f\\U_i\end{matrix}\right|}, \quad (1)$$

where U is the potential window (V) with U_i and U_f being the initial and final values, respectively, I is the current density (A/cm^2), and t is the discharge time (s). The obtained capacitance of the RGO electrode was 41.1 mF/cm^2, which is much higher than that of a pristine Au electrode (42.3 μF/cm^2).

To demonstrate the effect of RGO solid contact on a potentiometric performance, we selected a potassium ion as a target molecule because the concentration of potassium ion is an indicator for muscle cramps, hypokalemia, and hyperkalemia during exercise [25]. Two different ion-selective electrodes were prepared using a drop-casting method (Fig. 2b): (1) an Au electrode with an ISM (ISM/Au) and (2) an Au electrode with RGO solid contact and an ISM (ISM–RGO/Au). The roughness morphology was observed after surface modification of the Au electrode with RGO. The drop-casting of ISM fully covered the RGO surface. The measurement of potentiometric K^+ responses was performed in a two-electrode system using an ISM–RGO/Au sensing electrode and an Ag/AgCl reference electrode immersed in an electrolyte K^+ solution (Fig. 2c). The electromotive force (EMF) responses between ISM–RGO/Au and Ag/AgCl electrodes were recorded by decreasing the concentration of the K^+ solution from 1 M to 3.8 μM. The calibration curve of EMF versus log [K^+] was plotted in Fig. 2d. The ISM–RGO/Au electrode showed a linear slope of 53.34 mV/log[K^+] in a range of 250–0.06 mM, which is close to a Nernstian behavior. Based on the intersection of two slopes, the detection limit for ISM–RGO/Au was calculated to be − 4.24 log[K^+] (0.06 mM).

The repeatability of the ISM–RGO/Au electrode was tested by repeatedly measuring EMF responses during increasing and decreasing K^+ concentration (Fig. 3a). The ISM–RGO/Au electrode has almost the same sensitivities of 52.46 mV/log[K^+] and 53.44 mV/log[K^+] for the front and back directions (Fig. 3b). The maintained sensitivity with a

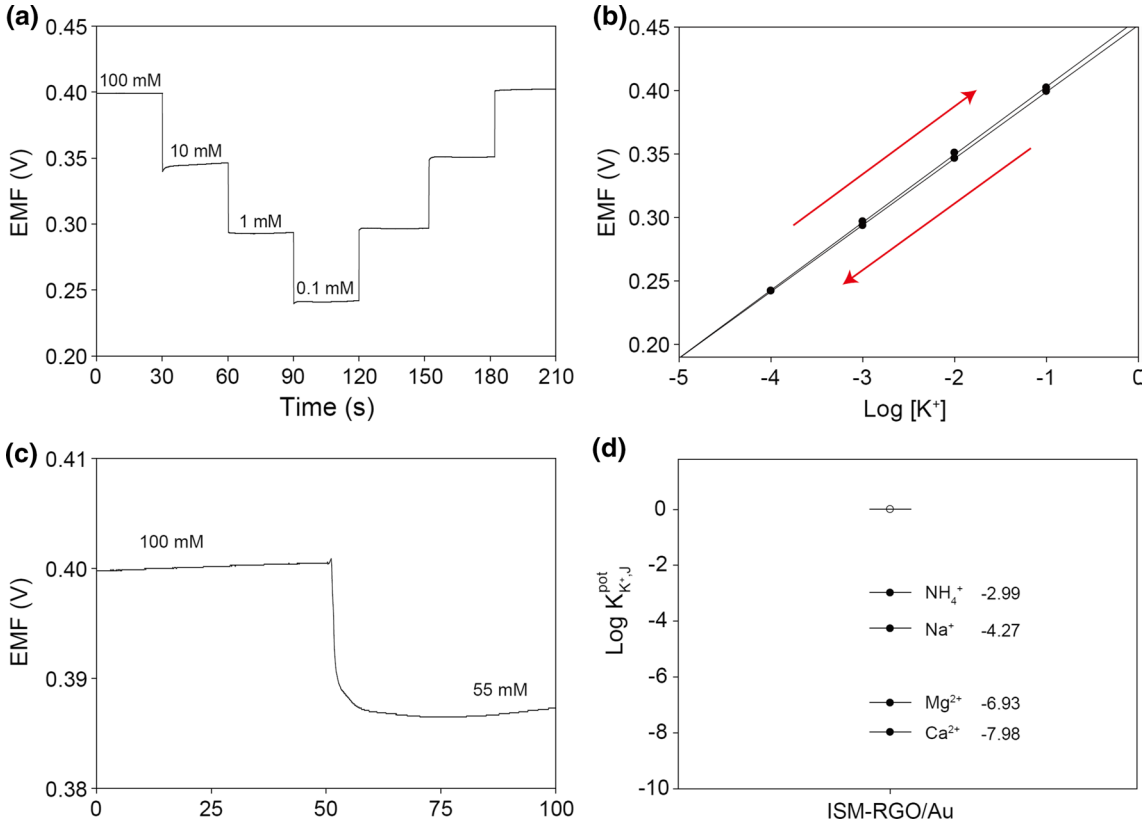

Fig. 3 **a** Hysteresis curve for the RGO/K^+–ISM electrode in varying potassium concentration solutions and **b** Linear relationship between EMF and log[K^+] with decreasing and increasing potassium concentration. **c** Change of EMF signals when diluting KCl solution from 100 to 55 mM. **d** Ion selectivity of ISM–RGO/Au electrode using separate solution method

small hysteresis width of 2.9 mV indicates good repeatability for the ISM–RGO/Au electrode. The ISM–RGO/Au electrode can spontaneously respond to the abrupt concentration change of the electrolyte solution within 6.0 s (Fig. 3c). This fast response time is essential for the high performance of all-solid-state ion sensors. The selectivity is also one of the most important characteristics for ISM electrodes (Fig. 3d). The selectivity coefficient ($K^{Pot}_{K^+,J}$) is a good indicator to determine an accurate measurement of a potassium ion in the presence of interfering ions (J) [26]. The selectivity coefficients were obtained using a separate solution method comparing the response of the ISM electrode to the primary ion and to that of the interfering ion. All of the selectivity coefficient values of ISM–RGO/Au electrodes to interfering ions of NH_4^+, Na^+, Mg^{2+}, and Ca^{2+} were below 1 (Fig. 3d), indicating a good selectivity of the ion-selective electrode.

The RGO–ISM/Au electrode showed excellent potential stability (Fig. 4). The potential stability against electrode polarization in a constant measuring condition can be investigated by measuring the capacitance of electrodes using a chronopotentiometric technique. The RGO–ISM/Au electrodes were charged and discharged at an applied constant current of ± 1 nA for 200 s. The potential stability based on the time (t) dependence of the electrode potential ($\Delta E/\Delta t$) can be expressed by the capacitance (C) of the electrode obtained at an applied constant current as following the equation [13]:

$$\text{Potential stability} = \Delta E/\Delta t = I/C \tag{2}$$

This equation indicates that as the capacitance increases, the potential responses become more stable. The specific capacitance (C_s) of electrodes can be calculated from chronopotentiometric charge/discharge curves using the following equation [27]:

$$C_s = I/(\Delta E/\Delta t), \tag{3}$$

where I is current density (A cm^{-2}), ΔE is a potential window after iR drop, and Δt is discharge time. The RGO–ISM electrode showed a symmetric charge/discharge curve, indicating ideal electrical double-layer capacitive behavior. The RGO–ISM electrode had a higher area capacitance of 2.38 mF/cm^2 and a lower potential drift (2 μV/s) than those of the Au–ISM electrode (0.10 mF/cm^2 and 50 μV/s). The high capacitance of the RGO–ISM electrode originated from a large surface area and electrical double-layer capacitance

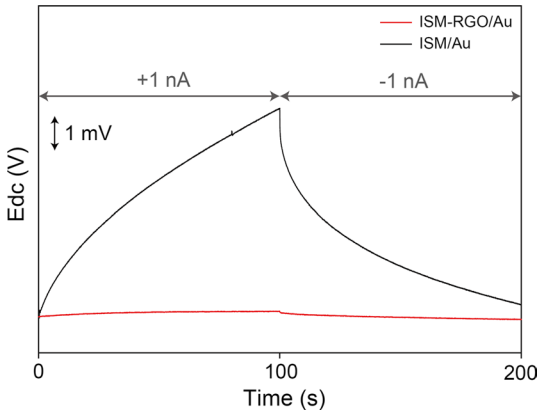

Fig. 4 Potential stability of ISM/Au and ISM–RGO/Au electrodes measured at an applied current of ±1 nA for 200 s in 0.1-M KCl solution

of RGO-enhanced potential stability compared to the Au–ISM electrode.

The formation of an unintentional water layer at the interface of the solid contact and the ISM is one of the most important criteria for the high potentiometric performance of ISM electrodes [28]. The diffusion of undesired ions or gases into water layer causes severe potential drifts and mechanical failure. The presence of the water layer was demonstrated by conditioning the ISM electrodes alternatively in solutions of the primary and interfering ions for a long time (Fig. 5) [29]. After being conditioned in a 0.1-M KCl solution overnight, EMF responses of ISM electrodes were measured by subsequently changing electrolyte ions from 0.1-M KCl (primary ions) to 0.1 NaCl (interfering ions) and back in initial primary ions of 0.1-M KCl. When the electrolyte ion returns to initial ion solution, the bare Au–ISM electrode showed unstable potential drift due to the presence of the water layer. In contrast, the RGO-based ISM electrode exhibited stable potential responses, which are close to its initial values. This result indicates that RGO solid contact enables the effective prevention of a water layer onto the surface of ISM because of the rough surface morphology and hydrophobic nature of RGO.

A good ISM electrode should endure interferences of light and gases (e.g., O_2, N_2, and CO_2), which are generally observed at conducting polymer-based ISM electrodes. The use of conducting polymer as a solid contact leads to a photosensitive electrode due to the organic semiconducting properties of conducting polymers [30]. The gas species can diffuse through the ISM and reach solid contact, resulting in the severe perturbation of potential measurement. The effect of light on the RGO–ISM electrode was tested by continuously measuring potential responses of the electrode during the ambient light on/off. In addition, the interferences of O_2, N_2, and CO_2 on potential measurement were investigated by bubbling these gases through electrolyte ion solutions. As shown in Fig. 6, RGO–ISM had no significant interferences against light and gases.

The highly selective potassium ion sensing performance of the RGO–ISM electrode with a good ion-to-electron transducer of RGO solid contact was applied for the fabrication of potassium ion sensor devices. Figure 7b shows the device configuration of a potentiometric K^+-sensor device, in which two electrodes are integrated with a printed circuit board (PCB). The PCB collects sensing data and transfers them to a notebook or a mobile phone. The digital data can also be displayed in a mobile application. The K^+-sensor consisted of a two-electrode system of RGO–ISM sensing and Ag/AgCl reference electrodes. The screen-printed process was used to fabricate electrode substrates of Ag-printed electrical circuits. This screen-printing technique allowed us to manufacture conductive patterns of electrodes in a large-scale, low-cost, and reproducible process. An Ag/AgCl reference electrode was prepared by electroless deposition of chloride and then

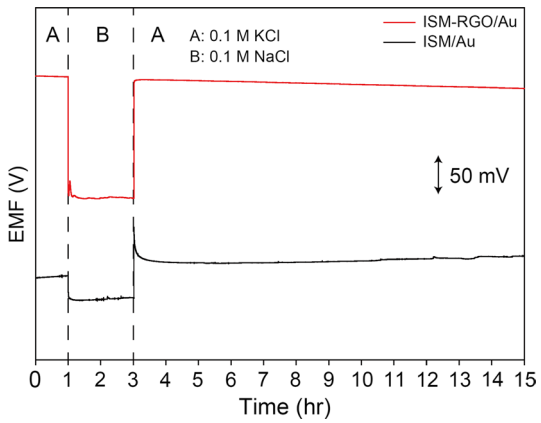

Fig. 5 Water layer tests of ISM/Au and ISM–RGO/Au electrodes in 0.1-M KCl (A) and 0.1-M NaCl (B) solutions

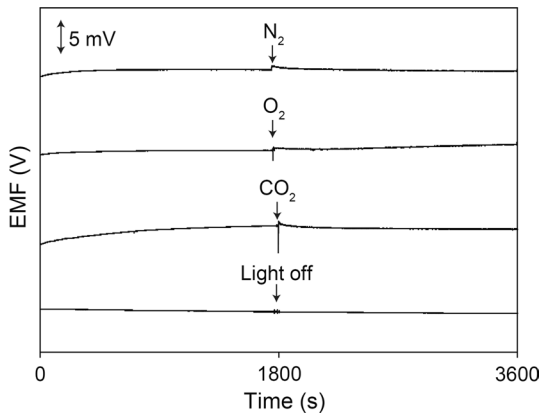

Fig. 6 EMF signals of ISM–RGO/Au electrode in 0.1-M KCl solution during N_2, O_2, CO_2 gas flows and under light on/off states

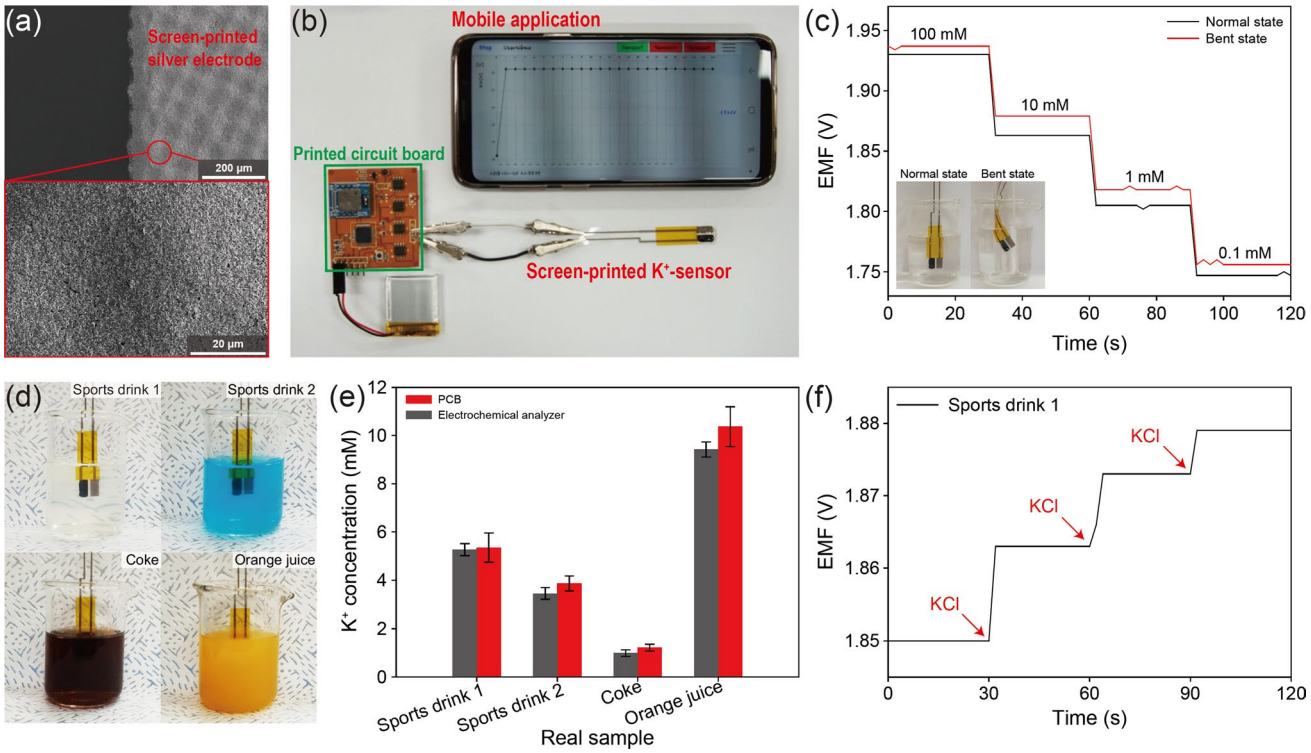

Fig. 7 **a** SEM image of screen-printed silver electrode. **b** Photograph image of screen-printed K^+-sensor integrated with PCB and mobile application. **c** EMF responses of K^+-sensor measured at a range of 100–0.1 mM of KCl solution under mechanically normal and bent states. Inset is photograph of K^+-sensor with normal and bent states. **d** Photograph images of K^+-sensor immersed in real samples of sports drink 1 (Pocari Sweat™), sports drink 2 (Powerade™), coke, and orange juice. **e** K^+ concentration of real samples using K^+-sensor using PCB and electrochemical analyzer. **f** EMF responses of K^+-sensor by adding 1-M KCl into sports drink 1

covering with PVB containing 78-mg NaCl. The RGO–ISM sensing electrode was prepared by subsequently drop-casting RGO and ISM onto the surface of the Ag electrode. The fabricated K^+-sensor spontaneously responded to exposing concentration changes in K^+ solutions by decreasing from 100 to 0.1 mM (Fig. 7c). The EMF responses were displayed in a mobile application, showing a sensitivity of 60.7 mV/log[K^+]. To demonstrate the feasibility of the K^+-sensor, real samples of sports drinks (sports drink 1: Pocari Sweat™ and sports drink 2: Powerade™), coke, and orange juice were measured, and the values were similar to those of an electrochemical analyzer (Fig. 7e). Furthermore, the K^+-sensor responded spontaneously to the change of ion concentration by adding 1-M KCl into sports drink 1 (Fig. 7f).

4 Conclusions

We prepared RGO hydrogels with a large surface and pore structure through the hydrothermal reduction of a GO solution. The electrical double-layer capacitive behavior and hydrophobicity of RGO made it an attractive solid contact between the potassium-selective membrane and Au electrode. The resultant ISM–RGO/Au electrode showed high sensitivity, a low detection limit, a fast response time, and good selectivity. The RGO solid contact-based electrode, compared to the bare Au electrode, enhanced potential stability and more effectively prevented the formation of a water layer and interferences of light and gases. Moreover, we fabricated a potentiometric K^+-sensor based on a screen-printed process, in which PCB was interconnected to collect data and transfer them to a mobile application. The potentiometric K^+-sensor performed accurate measurements of K^+ concentration in real samples of sports drinks, coke, and orange juice, which were consistent with an electrochemical analyzer. The potentiometric ion sensors based on RGO solid contact offers great promise for reliable and reproducible electrochemical performances of all-solid-state ion sensors.

Acknowledgements This research was supported by the Bio & Medical Technology Development Program of the National Research Foundation (NRF) and funded by the Korean government (MSIP) (Nos. 2015M3A9D7067457, 2018R1C1B3001553).

Compliance with ethical standards

Conflict of interest No potential conflict of interest relevant to this article was reported.

References

1. Hu J, Stein A, Bühlmann P (2016) Rational design of all-solid-state ion-selective electrodes and reference electrodes. TrAC Trends Anal Chem 76:102–144. https://doi.org/10.1016/j.trac.2015.11.004
2. Yang Y, Gao W (2018) Wearable and flexible electronics for continuous molecular monitoring. Soc Rev, Chem. https://doi.org/10.1039/c7cs00730b
3. Gao W, Emaminejad S, Nyein HYY, Challa S, Chen K, Peck A, Fahad HM, Ota H, Shiraki H, Kiriya D, Lien D, Brooks GA, Davis RW, Javey A (2016) Fully integrated wearable sensor arrays for multiplexed in situ perspiration analysis. Nature 529:509–514. https://doi.org/10.1038/nature16521
4. Parrilla M, Cánovas R, Jeerapan I, Andrade FJ, Wang J (2016) A textile-based stretchable multi-ion potentiometric sensor. Adv Healthc Mater 5:996–1001. https://doi.org/10.1002/adhm.201600092
5. Emaminejad S, Gao W, Wu E, Davies ZA, Nyein HYY, Challa S, Ryan SP, Fahad HM, Chen K, Shahpar Z, Talebi S, Milla C, Javey A, Davis RW (2017) Autonomous sweat extraction and analysis applied to cystic fibrosis and glucose monitoring using a fully integrated wearable platform. Proc Natl Acad Sci USA 114:4625–4630. https://doi.org/10.1073/pnas.1701740114
6. Hu J, Stein A, Bühlmann P (2016) A disposable planar paper-based potentiometric ion-sensing platform. Angew Chem Int Ed 55:7544–7547. https://doi.org/10.1002/anie.201603017
7. Ruecha N, Chailapakul O, Suzuki K, Citterio D (2017) Fully inkjet-printed paper-based potentiometric ion-sensing devices. Anal Chem 89:10608–10616. https://doi.org/10.1021/acs.analchem.7b03177
8. He Q, Das SR, Garland NT, Jing D, Hondred JA, Cargill AA, Ding S, Karunakaran C, Claussen JC (2017) Enabling inkjet printed graphene for ion selective electrodes with postprint thermal annealing. ACS Appl Mater Interfaces 9:12719–12727. https://doi.org/10.1021/acsami.7b00092
9. van de Velde L, d'Angermont E, Olthuis W (2016) Solid contact potassium selective electrodes for biomedical applications—a review. Talanta 160:56–65. https://doi.org/10.1016/j.talanta.2016.06.050
10. Yu K, He N, Kumar N, Wang N, Bobacka J, Ivaska A (2017) Electrosynthesized polypyrrole/zeolite composites as solid contact in potassium ion-selective electrode. Electrochim Acta 228:66–75. https://doi.org/10.1016/j.electacta.2017.01.009
11. Veder J, De Marco R, Patel K, Si P, Grygolowicz-Pawlak E, James M, Alam MT, Sohail M, Lee J, Pretsch E, Bakker E (2013) Evidence for a surface confined ion-to-electron transduction reaction in solid-contact ion-selective electrodes based on poly(3-octylthiophene). Anal Chem 85:10495–10502. https://doi.org/10.1021/ac4024999
12. Boeva ZA, Lindfors T (2016) Few-layer graphene and polyaniline composite as ion-to-electron transducer in silicone rubber solid-contact ion-selective electrodes. Sens Actuators B 224:624–631. https://doi.org/10.1016/j.snb.2015.10.054
13. Crespo GA, Macho S, Rius FX (2008) Ion-selective electrodes using carbon nanotubes as ion-to-electron transducers. Anal Chem 80:1316–1322. https://doi.org/10.1021/ac071156l
14. Fouskaki M, Chaniotakis N (2008) Fullerene-based electrochemical buffer layer for ion-selective electrodes. Analyst 133:1072–1075. https://doi.org/10.1039/B719759D
15. Hernández R, Riu J, Bobacka J, Vallés C, Jiménez P, Benito AM, Maser WK, Rius FX (2012) Reduced graphene oxide films as solid transducers in potentiometric all-solid-state ion-selective electrodes. J Phys Chem C 116:22570–22578. https://doi.org/10.1021/jp306234u
16. Ping J, Wang Y, Ying Y, Wu J (2012) Application of electrochemically reduced graphene oxide on screen-printed ion-selective electrode. Anal Chem 84:3473–3479. https://doi.org/10.1021/ac203480z
17. Hu J, Zou XU, Stein A, Bühlmann P (2014) Ion-selective electrodes with colloid-imprinted mesoporous carbon as solid contact. Anal Chem 86:7111–7118. https://doi.org/10.1021/ac501633r
18. Fierke MA, Lai CZ, Bühlmann P, Stein A (2010) Effects of architecture and surface chemistry of three-dimensionally ordered macroporous carbon solid contacts on performance of ion-selective electrodes. Anal Chem 82:680–688. https://doi.org/10.1021/ac902222n
19. Neto AHC, Guinea F, Peres NMR, Novoselov KS, Geim AK (2009) The electronic properties of graphene. Rev Mod Phys 81:109–162. https://doi.org/10.1103/RevModPhys.81.109
20. Pei S, Cheng H (2012) The reduction of graphene oxide. Carbon 50:3210–3228. https://doi.org/10.1016/j.carbon.2011.11.010
21. Bai H, Li C, Shi G (2011) Functional composite materials based on chemically converted graphene. Adv Mater 23:1089–1115. https://doi.org/10.1002/adma.201003753
22. Bariya M, Shahpar Z, Park H, Sun J, Jung Y, Gao W, Nyein HYY, Liaw TS, Tai L, Ngo QP, Chao M, Zhao Y, Hettick M, Cho G, Javey A (2018) Roll-to-roll gravure printed electrochemical sensors for wearable and medical devices. ACS Nano 12:6978–6987. https://doi.org/10.1021/acsnano.8b02505
23. Stankovich S, Dikin DA, Piner RD, Kohlhaas KA, Kleinhammes A, Jia Y, Wu Y, Nguyen ST, Ruoff RS (2007) Synthesis of graphene-based nanosheets via chemical reduction of exfoliated graphite oxide. Carbon 45:1558–1565. https://doi.org/10.1016/j.carbon.2007.02.034
24. Jeon H, Jeong J, Kang HG, Kim H, Park J, Kim DH, Jung YM, Hwang SY, Han Y, Choi BG (2018) Scalable water-based production of highly conductive 2D nanosheets with ultrahigh volumetric capacitance and rate capability. Adv Energy Mater 8:1800227. https://doi.org/10.1002/aenm.201800227
25. Lindinger MI, Sjøgaard G (1991) Potassium regulation during exercise and recovery. Sports Med 11:382–401. https://doi.org/10.2165/00007256-199111060-00004
26. Maccá C (2003) The current usage of selectivity coefficients for the characterization of ion-selective electrodes. A critical survey of the 2000/2001 literature. Electroanalysis 15:997–1010. https://doi.org/10.1002/elan.200390129
27. Hong SB, Jeong J, Kang HG, Seo D, Cha Y, Jeon H, Lee GY, Irshad M, Kim DH, Hwang SY, Kim JW, Choi BG (2018) Fast and scalable hydrodynamic synthesis of MnO_2/defect-free graphene nanocomposites with high rate capability and long cycle life. ACS Appl Mater Interfaces 10:35250–35259. https://doi.org/10.1021/acsami.8b12894
28. Fibbioli M, Morf WE, Badertscher M, De Rooij NF, Pretsch E (2000) Potential drifts of solid-contacted ion-selective electrodes due to zero-current ion fluxes through the sensor membrane. Electroanalysis 12:1286–1292. https://doi.org/10.1002/1521-4109(200011)12:16%3c1286:AID-ELAN1286%3e3.0.CO;2-Q
29. Bakker E, Bühlmann P, Pretsch E (2004) The phase-boundary potential model. Talanta 63:3–20. https://doi.org/10.1016/j.talanta.2003.10.006
30. Vázquez M, Bobacka J, Ivaska A, Lewenstam A (2002) Influence of oxygen and carbon dioxide on the electrochemical stability of poly(3,4-ethylenedioxythiophene) used as ion-to-electron transducer in all-solid-state ion-selective electrodes. Sens Actuators B 82:7–13. https://doi.org/10.1016/S0925-4005(01)00983-2